

2012

Growth Analysis of (Ag,Cu)InSe₂ Thin Films Via Real Time Spectroscopic Ellipsometry

S. A. Little

V. Ranjan
Old Dominion University

R. W. Collins

S. Marsillac
Old Dominion University, Smarsill@odu.edu

Follow this and additional works at: https://digitalcommons.odu.edu/ece_fac_pubs

 Part of the [Materials Science and Engineering Commons](#), and the [Optics Commons](#)

Repository Citation

Little, S. A.; Ranjan, V.; Collins, R. W.; and Marsillac, S., "Growth Analysis of (Ag,Cu)InSe₂ Thin Films Via Real Time Spectroscopic Ellipsometry" (2012). *Electrical & Computer Engineering Faculty Publications*. 21.
https://digitalcommons.odu.edu/ece_fac_pubs/21

Original Publication Citation

Little, S.A., Ranjan, V., Collins, R.W., & Marsillac, S. (2012). Growth analysis of (Ag,Cu)InSe₂ thin films via real time spectroscopic ellipsometry. *Applied Physics Letters*, 101(23 (231910)), 1-4. doi: 10.1063/1.4769902

Growth analysis of (Ag,Cu)InSe₂ thin films via real time spectroscopic ellipsometry

S. A. Little, V. Ranjan, R. W. Collins, and S. Marsillac

Citation: [Applied Physics Letters](#) **101**, 231910 (2012); doi: 10.1063/1.4769902

View online: <http://dx.doi.org/10.1063/1.4769902>

View Table of Contents: <http://scitation.aip.org/content/aip/journal/apl/101/23?ver=pdfcov>

Published by the [AIP Publishing](#)

Articles you may be interested in

[Properties of Cu\(In,Ga,Al\)Se₂ thin films fabricated by magnetron sputtering](#)

J. Vac. Sci. Technol. A **33**, 031201 (2015); 10.1116/1.4913863

[Structural and optical properties of \(Ag,Cu\)\(In,Ga\)Se₂ polycrystalline thin film alloys](#)

J. Appl. Phys. **115**, 223504 (2014); 10.1063/1.4880243

[Nanostructured light-absorbing crystalline CuIn\(1-x\)Ga_xSe₂ thin films grown through high flux, low energy ion irradiation](#)

J. Appl. Phys. **114**, 153505 (2013); 10.1063/1.4823987

[Electronic and structural properties of molybdenum thin films as determined by real-time spectroscopic ellipsometry](#)

Appl. Phys. Lett. **94**, 141908 (2009); 10.1063/1.3117222

[Quasi real-time Raman studies on the growth of Cu-In-S thin films](#)

J. Appl. Phys. **95**, 5153 (2004); 10.1063/1.1667009

The advertisement features a blue background with a molecular structure of spheres. On the left is a thumbnail of an 'Applied Physics Reviews' journal cover showing a diagram of a layered structure. The main text reads 'NEW Special Topic Sections' in large white font. Below this, it says 'NOW ONLINE' in yellow, followed by 'Lithium Niobate Properties and Applications: Reviews of Emerging Trends' in white. The AIP Applied Physics Reviews logo is in the bottom right corner.

NEW Special Topic Sections

NOW ONLINE
Lithium Niobate Properties and Applications:
Reviews of Emerging Trends

AIP Applied Physics Reviews

Growth analysis of (Ag,Cu)InSe₂ thin films via real time spectroscopic ellipsometry

S. A. Little,¹ V. Ranjan,^{2,a)} R. W. Collins,¹ and S. Marsillac^{2,b)}

¹Department of Physics and Astronomy, University of Toledo, Toledo, Ohio 43606, USA

²Department of Electrical and Computer Engineering, Old Dominion University, Norfolk, Virginia 23525, USA

(Received 16 June 2012; accepted 20 November 2012; published online 7 December 2012)

In situ and *ex situ* characterization methods have been applied to investigate the properties of (Ag,Cu)InSe₂ (ACIS) thin films. Data acquired from real time spectroscopic ellipsometry (RTSE) experiments were analyzed to extract the evolution of the nucleating, bulk, and surface roughness layer thicknesses. The evolution of these layer thicknesses suggests a transition from Volmer-Weber to Stranski-Krastanov type behavior when Cu is replaced by Ag. The complex dielectric functions of ACIS at both deposition and room temperature as a function of film composition were also extracted from the RTSE data, enabling parameterization of the alloy optical properties.

© 2012 American Institute of Physics. [<http://dx.doi.org/10.1063/1.4769902>]

The achievement of maximizing the efficiency of solar cells from the Cu(In,Ga)Se₂ quaternary alloy system to 20.3%, through group III isoelectronic substitution of In by Ga,¹ leads one to believe that a similar benefit may be possible by group I substitution. Given its many optically reactive chalcogenide compounds, Ag is of great interest as a substitute for Cu. Recently, solar cell devices with optimized Ag content in (Ag,Cu)(In,Ga)Se₂ have been reported,^{2,3} and *ex situ* spectroscopic ellipsometry (SE) studies of (Ag,Cu)(In,Ga)Se₂ (ACIGS) thin films have also been reported.⁴ The SE studies of Ref. 4 were performed at room temperature (RT) and span the photon energy range of 0.5–4.7 eV. In the present article, results of *in situ* real time SE (RTSE) measurements over the photon energy range of 0.75–6.5 eV are described for analysis of the nucleation and growth of (Ag,Cu)InSe₂ (ACIS) thin films. Models representing the dielectric function critical points as oscillators were used to extract important optical parameters including band gap and associated broadening energies. The effects of composition on the nucleation, coalescence, and grain growth processes have been characterized, as these processes control the ultimate film morphology and grain structure.

ACIS films 500 nm thick were deposited by dc magnetron sputtering at a substrate temperature of $T_s = 550^\circ\text{C}$ onto Si (100) wafers with 25 nm thermal oxides. High purity targets of Ag, Cu, and In were sputtered in argon gas (99.998%), which was maintained at a pressure of 2.5 mTorr. The dc power levels of the targets were independently controlled and were varied from run to run in order to obtain films of varying ratio of Ag to total Group I atoms, $w = [\text{Ag}]/([\text{Cu}] + [\text{Ag}])$. Selenium was evaporated at a constant rate simultaneously with Ag, Cu, and In sputtering. RTSE data were acquired *in situ* during film growth using a rotating-compensator multichannel ellipsometer with the 0.75–6.5 eV photon energy range at an angle of incidence of 65° . The optical model of the growing ACIS film used in

data analysis is based on a two-layer structure consisting of surface roughness and bulk layers of thicknesses d_s and d_b , respectively, on the fully characterized SiO₂/Si wafer substrate.⁵ In the absence of a bulk layer, i.e., for d_b less than a single monolayer (~ 0.5 nm), the surface roughness layer of thickness d_s was interpreted as the nucleating layer. The dielectric functions of the nucleating and surface roughness layers were simulated using the Bruggeman effective medium approximation (EMA)⁶ assuming a mixture of void and bulk ACIS. The experimental spectra in ψ and Δ were fit assuming the two-layer roughness/bulk model as described and using an iterative combination of least squares regression for the structural parameters and numerical inversion for the dielectric function, as described in detail elsewhere.^{5,6} The weak uniaxial optical anisotropy of ACIS due to its chalcopyrite crystal structure (tetragonal system) was neglected since the polycrystallinity of the films makes its detection problematic.

Complementary *ex situ* characterization of the as-deposited ACIS films included x-ray diffractometry (XRD), scanning electron microscopy (SEM) with energy dispersive spectroscopy (EDS), and Auger electron spectroscopy (AES). Assignment of the XRD peaks yielded results consistent with the single phase chalcopyrite crystal structure. The composition of each ACIS film was confirmed by EDS and XRD assuming Vegard's Law; similar results were found and reported previously.³ AES depth profiles were obtained throughout the thickness of the films and demonstrated the absence of compositional depth gradients.

Figure 1(a) depicts the growth parameters that describe the first 50 nm of deposition as a function of the effective thickness, given by $d_{\text{eff}} = d_b + f_s d_s$, where f_s is the volume fraction of ACIS in the layer of thickness d_s . The effective thickness is equivalent to the total volume of ACIS per unit area of substrate. From the *in situ* RTSE analysis yielding (d_b , d_s), variations in the structural evolution were identified depending on the Ag content. In previous studies of sputtered CdTe films deposited in a similarly designed deposition/measurement system, the sensitivity and reproducibility of these measurements on sub-monolayer scales (± 0.05 nm) were

^{a)}Permanent address: Pilkington North America, Northwood, Ohio 43619, USA

^{b)}Author to whom correspondence should be addressed. Electronic mail: smarsill@odu.edu.

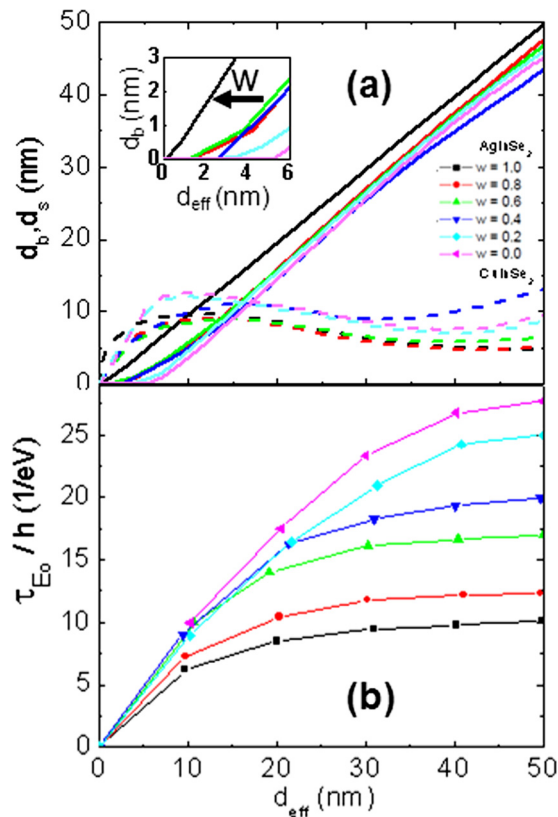


FIG. 1. (a) (Top) Bulk layer thickness (d_b) (solid lines) and surface roughness (or nucleating layer) thickness (d_s) (dashed lines) vs. effective thickness during the first 50 nm of deposition for films of different Ag content w . The inset shows a magnified view of d_b in the early nucleation stage, whereby the arrow denotes decreasing d_{eff} (i.e., decreasing d_s) at fixed d_b as w increases. (b) (Bottom) Inverse of the broadening parameter $1/\Gamma_{E_0}$ for the E_0 band gap as a function of effective thickness for films of different Ag content w .

demonstrated.⁵ In the present study, for all film compositions containing Cu ($w < 1$), a nucleating layer of thickness d_s appears before the formation of the first bulk density monolayer (approximated as $d_b \sim 0.5$ nm). This behavior is suggestive of initial island formation or the Volmer-Weber (V-W) nucleation mode.⁷ For AgInSe₂ (AIS) with $w = 1$ in Fig. 1(a), however, the growth of a bulk-like monolayer appears first, followed by island formation, or a Stranski-Krastanov (S-K) type growth mode.⁷ This behavior has also been observed in RTSE measurements of CdTe for $T_s > 0.4T_m$ (in K), where T_m is the melting temperature.⁵ The nucleation data summarizing Fig. 1(a) are depicted in Fig. 2, which shows the surface roughness thickness at which the underlying “bulk-like” layer reaches $d_b \sim 0.5$ nm. Also shown in this figure is the maximum nucleating layer thickness, which represents the cluster height prior to coalescence. Stronger substrate adhesive bonding for AgInSe₂ compared to film cohesive bonding can explain the growth mode behavior of Fig. 2 (triangles), consistent with the much lower AgInSe₂ melting point. After the first monolayer forms and coalesces, however, the accumulation of strain in the bulk-like layer may reverse the growth mode to islanding.⁷

The same ellipsometric spectra (ψ , Δ) used in determining the growth parameters were also applied to extract the dielectric functions $\varepsilon = \varepsilon_1 + i\varepsilon_2$ at different thicknesses. The results shown in Fig. 3 for ACIS films at the deposition temperature (550 °C) were obtained *in situ* by RTSE after

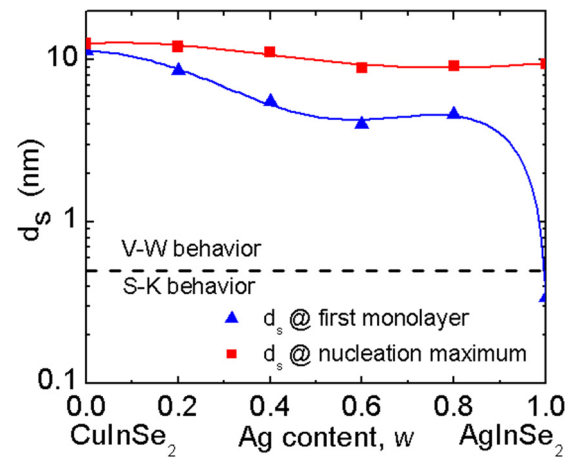


FIG. 2. The surface roughness layer thickness d_s at the onset of bulk layer formation (i.e., when $d_b \sim 0.5$ nm) plotted as a function of Ag content w . Also shown is the maximum nucleating or roughness layer thickness during nucleation.

stabilization of the dielectric functions versus thickness. As described below, this stabilization may occur when the grain size no longer increases (or coarsens) with thickness. In addition, at sufficiently large grain sizes, e.g., for low w , the relaxation time due to grain boundary or defect scattering may exceed that due to phonon scattering. Such an effect may also lead to a stabilization of the dielectric function with thickness. These stabilized dielectric functions were modeled using parabolic band oscillators⁸ at the critical points in order to extract more accurate information regarding the thickness evolution of the band gaps, as well as that of the broadening parameters, for films of the different values of w . The relevant expression is

$$\varepsilon(E) = \varepsilon_\infty + \sum_n A_n e^{i\theta_n} (E - E_n + i\Gamma_n)^{\mu_n}, \quad (1)$$

where ε_∞ is the real dielectric function offset, A_n is the amplitude, E_n is the resonance energy, Γ_n is the broadening

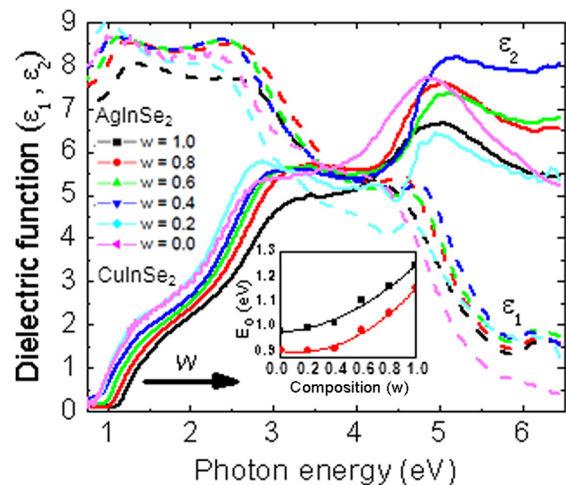


FIG. 3. Dielectric functions for ACIS films of different Ag content w deposited at 550 °C. The arrow for ε_2 (near the band gap) indicates the direction of increasing Ag content. The inset shows the band gap of ACIS at room temperature (squares) and at 550 °C (circles) as a function of Ag content w . Polynomial fits (solid lines) provide the bowing parameters.

parameter, and θ_n and μ_n are the phase and exponent of the transition.

Plotted in the inset of Fig. 3 and tabulated in Table I are the fundamental E_0 band gaps E_g as functions of composition for deposition and room temperatures. The band gap is found to shift to higher energy as the Ag content w increases at both temperatures. The room temperature values are in good agreement with those found by Albornoz *et al.*,⁴ and as expected, the band gaps decrease with increasing temperature. The agreement between the two sets of room temperature data in Table I (i.e., to within ± 0.015 eV) suggest that composition w is the key determinant of the band gap. Strain is not believed to be a significant effect since it is unlikely that films prepared in different laboratories have identical strain levels as well as strain variations with composition. The bowing parameter calculated from the SE room temperature data of the present study is 0.23 (in close agreement with the value of 0.22 reported by Albornoz *et al.*⁴), whereas the bowing parameter at 550 °C is larger at 0.33. This high temperature bowing parameter, along with the endpoint band gaps, are very useful as they allow one to determine the composition of a specific ACIS thin film in real time and *in situ* during the 550 °C deposition process though determination of the band gap. This in turns allows for a modification of the deposition process if an undesired deviation from the standard recipe is observed (i.e., monitoring) or if a desired gradient in the band gap is sought (i.e., control).

Referring again to Fig. 3, the amplitude of the step in ε_2 at the E_0 band gap E_g , decreases as Ag is incorporated, i.e., as w increases. In single crystals, such a decrease may derive from the proportionality $\varepsilon_2(E) \propto E^{-2} \Sigma_{cv} P_{cv}(E) J_{cv}(E)$,⁸ due to the increase in E_g with w , in conjunction with constant matrix element $P_{cv}(E \sim E_g)$ and joint density of states $J_{cv}(E \sim E_g)$ values. As previously calculated, a replacement of Cu by Ag results in a small increase in reduced effective mass, m^* .⁹ This increase in m^* also increases J_{cv} , but with an insignificant influence on the ε_2 step amplitude. The room temperature band gap values for AgInSe₂ and CuInSe₂ reported here, along with the literature conduction band effective masses,⁹ would lead to nearly the same value of $2P_{cv}^2/m_e \sim 10.5$ eV upon application of $\mathbf{k}\cdot\mathbf{p}$ theory,⁸ where m_e is the electron mass. Thus, a near constant P_{cv} is supported as well. In addition to the E^{-2} factor, voids in polycrystalline films may also decrease the ε_2 step amplitude. Voids may evolve at $w = 1$ in particular, due to the stress associated with the S-K growth mechanism, an effect observed previously in CdTe.⁵

Since the nucleation behavior in the initial stage of the deposition of polycrystalline semiconductors has been observed to impact the subsequent structural evolution of the

film and the ultimate material properties,⁵ the evolution of the broadening parameter Γ_{E_0} of the fundamental band gap critical point E_0 was also studied as a function of w . Previous studies of nanocrystalline and polycrystalline semiconductor films have suggested that the inverse of the increase in broadening over the single crystal value is proportional to the grain size, assuming that the grain boundary scattering controls the broadening.^{10,11} The basic equation is as follows:

$$\frac{hv_g}{R} = \Gamma_{E_0} - \Gamma_b, \quad (2)$$

where R is the grain radius, Γ_b is the single crystal E_0 broadening parameter, and v_g is the carrier group velocity, which is determined by the most mobile carrier. Neglecting Γ_b since it is often quite small for the E_0 transition leads to the simple expression $\tau_{E_0}/h \sim 1/\Gamma_{E_0} \sim R/hv_g$.

Figure 1(b) shows a monotonic increase in τ_{E_0}/h with thickness that can be attributed to an increase in grain size R as the film structure evolves, in accordance with Eq. (2). The clear trends as a function of alloy content are also of interest. Although the group velocity may vary for the alloy series, the reported increase in the conduction band effective mass from CuInSe₂ (CIS) to AIS⁹ would be expected to lead to a decreased v_g and thus an increase in τ_{E_0}/h for a given grain size. Thus, Fig. 1(b) indicates that the grain size decreases continuously with w from CIS to AIS irrespective of the thickness, and that the grain growth tends to saturate faster for the Ag-rich alloys. Although various physical attributes can affect the scattering process, such as point and line defects and even stress, it is believed that the grain size broadening mechanism limits the electron mean free path; this hypothesis is supported both by XRD and by cross sectional SEM results.³ Because of the reduced grain size in the Ag-rich alloys, the potential exists for growth engineering of these ACIS thin films by developing multi-stage processing analogous to the two-stage and three-stage processes used in conventional Cu(In,Ga)Se₂ solar cells.¹² This may also result in unintended alloy compositional non-uniformity with depth, which can be controlled as well to establish desired profiles for optimum device performance.

In conclusion, (Ag,Cu)InSe₂ thin films were grown by a hybrid sputtering/evaporation process and were characterized by *in situ* RTSE and *ex situ* XRD, SEM, EDS, and AES. RTSE has been applied to investigate the structural evolution and dielectric functions of these films. Changes in the growth process occur from V-W to S-K behavior with the replacement of Cu by Ag to yield AgInSe₂. This appears to occur due to a reduction in the cohesive energy of the film relative to its adhesive energy to the substrate, possibly also reflected in the reduction in melting temperature of AgInSe₂. In addition, the grain size is observed to increase with increasing thickness in all alloys, but saturating more quickly at a smaller grain size in the Ag-rich alloys, indicating either a decrease in grain size or increase defect density or disorder in the Ag-rich alloys. The dielectric functions extracted in the same analysis provide a fingerprint of alloy composition; and in particular, extraction of the fundamental band gap from the dielectric function measured at the deposition temperature enables compositional determination under actual growth

TABLE I. Fundamental band gaps ($E_g = E_0$) for ACIS films of various compositions w at RT and at 550 °C. Also shown for comparison are the results from Ref. 4.

$w = [\text{Ag}]/([\text{Cu}] + [\text{Ag}])$	1.0	0.8	0.6	0.4	0.2	0.0
E_g (RTSE 550 °C)	1.15	1.05	0.98	0.91	0.90	0.90
E_g (RTSE RT)	1.24	1.16	1.10	1.01	0.99	0.98
E_g ([Albornoz 2005] RT)	1.22	1.16	1.09	1.03	1.01	1.01

conditions. This methodology can serve as an effective tool in the future for (Ag,Cu)InSe₂ band gap engineering.

- ¹P. Jackson, D. Hariskos, E. Lotter, S. Paetel, R. Wuerz, R. Menner, W. Wischmann, and M. Powalla, *Prog. Photovoltaics* **19**, 894 (2011).
- ²G. M. Hanket, J. H. Boyle, and W. N. Shafarman, in *34th IEEE PVSC* (2009), p. 001240.
- ³S. Little, V. Ranjan, R. W. Collins, and S. Marsillac, in *38th IEEE PVSC* (2012), p. 000886.
- ⁴J. G. Albornoz, R. Serna, and M. León, *J. Appl. Phys.* **97**, 103515 (2005).
- ⁵S. Marsillac, M. N. Sestak, J. Li, and R. W. Collins, in *Advanced Characterization Techniques for Thin Film Solar Cells*, edited by D. Abou-Ras, T. Kirchartz, and U. Rau, (Wiley-VCH, Weinheim, Germany, 2011), Chap. 6, p. 125.
- ⁶H. Fujiwara, J. Koh, P. I. Rovira, and R. W. Collins, *Phys. Rev. B* **61**, 10832 (2000).
- ⁷J. A. Venables, *Introduction to Surface and Thin Film Processes* (Cambridge University, New York, 2000), p. 146.
- ⁸P. Y. Yu and M. Cardona, *Fundamentals of Semiconductors*, 3rd ed. (Springer, Berlin, 2005), Chap. 2 and 6.
- ⁹T. Omata, K. Nose, and S. Otsuka-Yao-Matsuo, *J. Appl. Phys.* **105**, 073106 (2009).
- ¹⁰J. Li, J. Chen, and R. W. Collins, *Appl. Phys. Lett.* **97**, 181909 (2010).
- ¹¹H. V. Nguyen and R. W. Collins, *Phys. Rev. B* **47**, 1911 (1993).
- ¹²W. N. Shafarman and L. Stolt, "Chapter 13: Cu(In,Ga)Se₂," in *Handbook of Photovoltaic Science and Engineering*, edited by A. Luque and S. Hegedus (Wiley, Chichester, UK, 2003).